DUAL-ENERGY SUBTRACTION TOMOSYNTHESIS – SIMULATION STUDIES USING A 3D BREAST SOFTWARE PHANTOM

K. Bliznakova, Z. Kolitsi and N. Pallikarakis

Department of Medical Physics, School of Medicine, University of Patras, 26500, Rio, Patras, GREECE

nipa@bme.med.upatras.gr

Abstract: This paper demonstrates the feasibility of using combined application of dual-energy and Digital Tomosynthesis (DTS) techniques in the case of mammography. This has been achieved in an extensive comparison between results demonstrated in simulated (a) conventional mammography; (b) conventional dual-energy mammography (DEM); (c) DTS and (d) combined DEM-DTS using 3D breast software phantoms. Our investigation demonstrated that the combination of DEM and Tomosynthesis results in significantly improved microcalcification visibility and useful 3D lesion information.

Introduction

X-ray mammography is the most important screening tool for breast carcinoma. It is estimated to detect on average 85% of the early diagnosed breast cancers [1]. Despite recent improvements in the mammography equipment and reported imaging techniques, the radiographs of dense breasts are still difficult to interpret [2]. Over the last two decades, the potential of the dual-energy mammography (DEM) for detection of small calcifications and microcalcifications (μC) has been investigated in a number of theoretical and experimental studies [3-9]. These investigations converge on the potential of DEM techniques to enhance breast image diagnostic value. Mammography and DEM, however are techniques related to a planar presentation of the 3D breast information. It has been shown that due to this planar presentation, "missed" carcinomas are often the case in radiographically dense breasts.

An improvement in interpretering the obtained images will come from further applying imaging techniques and methods to obtain precise 3D μC information. This has lead to the introduction of Tomosynthesis as an advanced breast imaging technique [10, 11]. Studies, performed with this technique already indicated the improved cancer delectability, as well as the improved lesion visibility and image projection contrast [12]. Few works on dual-energy tomosynthesis have been reported in the past as well [13, 14]. They reported applications of this combination in the area of the chest and vascular imaging. These investigations concluded the feasibility of dual-energy techniques with tomosynthesis in the enhancing pulmonary lesions and reconstructions of vascular threes.

We have carried out a number of simulation studies with the objective to investigate possible further improvement in μC detection, which could result from a combined application of DEM and digital tomosynthesis (DTS) techniques. This combination is denoted as DEM-DTS. This has been achieved in an extensive comparison between results demonstrated in (a) conventional mammography; (b) conventional DEM; (c) DTS and (d) combined DEM-DTS using 3D breast software phantoms and software simulators that simulate these imaging techniques [15]. The studies were limited to incident monoenergetic beams. Our investigation demonstrated significantly improved visibility of μC and accurate 3D lesion information in the tomograms obtained by DEM-DTS technique.

Materials and Methods

The approach we followed, involved the design of breast phantoms with fatty, fatty-glandular and dense tissues and clusters of μCs, generated randomly in the models. Subsequently, these breast models were used in simulations including conventional mammography, conventional DEM, DTS and DEM-DTS in order to generate a set of diagnostic images, subjected to multiple evaluations.

Breast phantoms. Breast phantoms with fatty, glandular and dense breast tissues were generated with dimensions, approximating small size breasts [15].

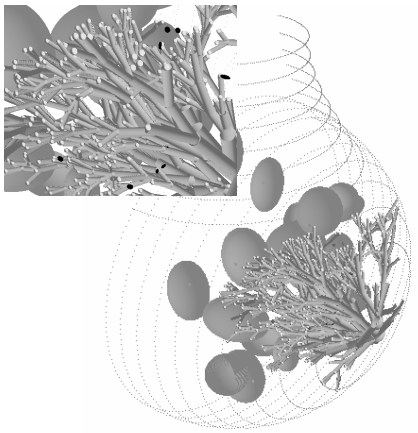

Figure 1: Breast phantom with 9 μC.

ISSN: 1727-1983

Figure 1 shows an example of one of the models used in the simulations, including 9 μC. The breast phantoms were synthesized to include a cluster of μC, modelled as $CaCO_3$ with size in the range 100 to 800 μm.

Simulation techniques. The following imaging acquisition techniques were simulated: (a) conventional mammography; (b) conventional DEM; (c) DTS and (d) DEM-DTS. Photon fluences and entrance skin exposures were calculated for each simulated acquisition technique and listed in Table 1. The entrance skin exposure is given per acquired image.

Conventional mammography simulation. Figure 2 shows the geometry of the imaging process for 3D mammography. The acquired image corresponded to cranio-caudial (CC) images. SOD and SDD are the distances from the source to the breast phantom and to the detector planes, respectively. These distances were set equal to 540 mm and 800 mm respectively. Monochromatic 18 keV beams emerge from a point source, at a distance SOD from the object plane, and penetrate the breast phantom. Photon transport is calculated as described in [15]. The images were acquired with size of 1024 x 1024 pixels, covering the synthesized breast phantoms. The stationary detector was modeled as BaFBr (98mg cm^{-2}) with resolution of 10 pixels/mm.

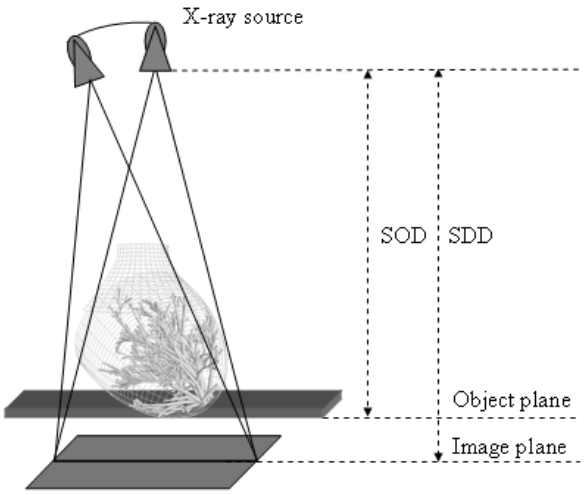

Figure 2: Graphical representation of simulated acquisition geometry.

DEM simulation. The incident 'low' and 'high' monoenergetic photon beams were with energies 18 keV and 47 keV, respectively. The acquired images corresponded to CC images. The simulated low and high energy images were subtracted according to the Ergun's formalism [16] (with R = 0.298) in order to obtain DEM images. The remaining geometry characteristics were as those described in the previous paragraph.

DTS application. DTS is a method of limited angle reconstruction of tomographic images produced at variable heights, on the basis of a set of angular projections. The simulated acquisition geometry included rotation of the x-ray source in an arc above the breast, while the breast phantom and the detector remained stationary (Figure 2). The simulated imaging protocol used 7 synthetic images acquired at 6^0 increments from -18^0 to 18^0 for 18 keV incident energy beam. Tomograms were reconstructed using the Multiple Projection Algorithm (MPA) [17].

DEM-DTS application. The simulated imaging protocol used 7 synthetic images acquired at 6^0 increments from -18^0 to 18^0 for both, the low and high energy beams. Subsequently, DEM images of each pair images were produced. Tomograms were reconstructed using the MPA applied on the obtained 7 DEM images.

Table 1: Simulation parameters for image acquisition.

Simulated technique	Total number of acquired images	Photons/pixel	Entrance skin exposure mR
CM	1 LE	3.299393E+5	800
DEM	1 LE	2.474544E+5	600
	1 HE	5.153999E+5	200
DTS	7 LE	4.714007E+4	114.3
DEM-DTS application	7 LE	3.534474E+4	85.7
	7 HE	7.370218E+4	28.6

LE - Low energy image; HE - High energy image; CM – conventional mammography

Evaluation Results

Synthetic mammographic images, obtained with ordinary and DEM mammography, and reconstructed tomograms, obtained with DTS and DEM-DTS technique were evaluated qualitatively by means of their visual assessment. Additionally, quantitative comparison was accomplished by calculating the μC Subject Contrast (SC). In case of DEM-DTS, the 3D locations and dimensions of the reconstructed μC were compared with their true values.

Figure 3a, b show synthetic mammograms of a fatty breast model, obtained using conventional mammography and DEM. Figure 3c, d show regions with μCs from tomograms, reconstructed using DTS technique applied on 7 LE images and 7 DEM images, respectively.

Figure 4a, b show the conventional and DEM images obtained using dense breast phantom, while some results from the DTS and DEM-DTS techniques are presented in Figure 4c, d.

ISSN: 1727-1983

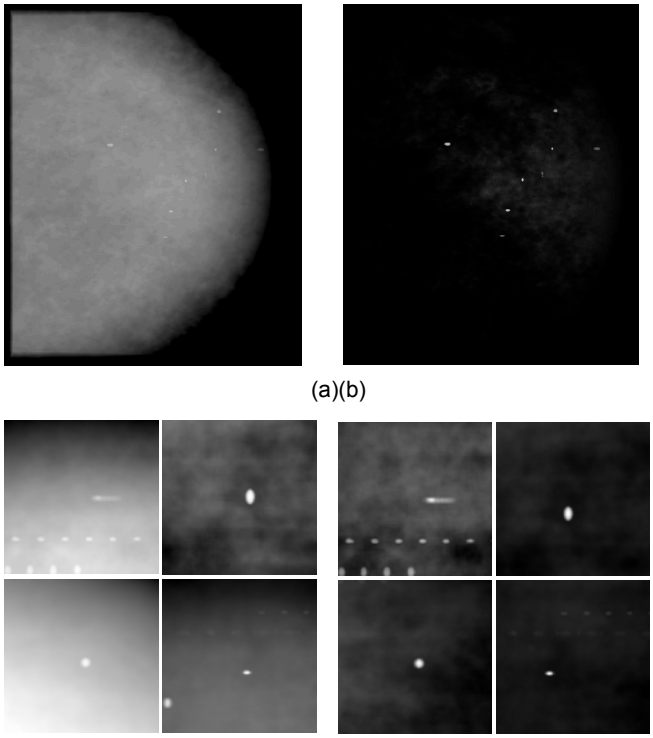

(a)(b)

(c)(d)

Figure 3: Synthetic mammograms obtained with (a) conventional mammography, (b) DEM, (c) DTS and (d) DEM-DTS.

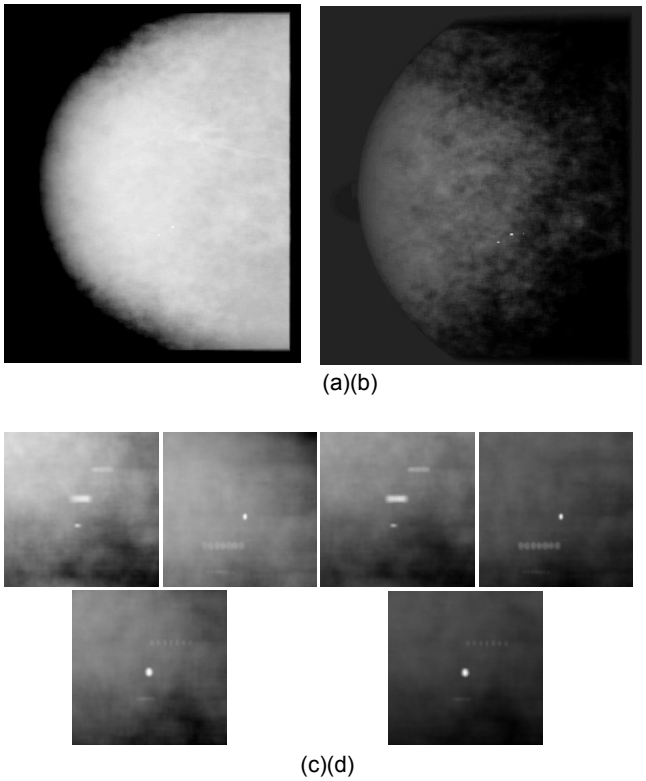

(a)(b)

(c)(d)

Figure 4: Synthetic mammograms of a dense breast model obtained with (a) conventional mammography, (b) DEM, (c) DTS and (d) DEM_DTS.

The 3D locations of the reconstructed μC were compared with their true values and presented in Figure 5. Additionally, the simulated techniques were compared by means of calculating the SC of each μC on the images under comparison. Data for the shown μC cases are displayed in Table 2.

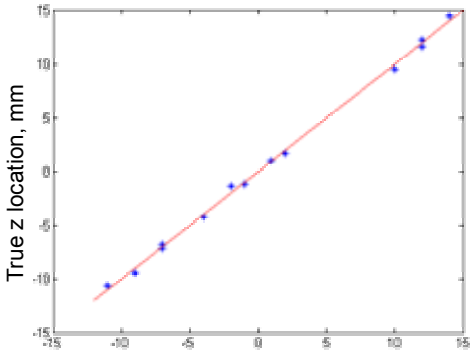

Figure 5: Comparison of depth locations of the reconstructed uCs.

Table 2: SC of the μCs on synthetic conventional mammogram (CM); DEM mammogram, DTS and DEM-DTS reconstructed slices.

	SC_{CM},%	SC_{DEM},%	SC_{DTS},%	$SC_{DEM-DTS}$,%
fatty	23.3754	53.9535	23.0818	70.2725
	22.7213	57.3054	255.3673	427.2917
	11.7780	13.0771	27.7984	219.2750
	25.2082	29.4040	152.8490	767.4969
dense	24.1302	53.6290	52.3923	74.5660
	14.8318	43.7502	64.1270	92.4542
	6.6486	10.2960	107.6756	127.9906

Discussion

The visual inspection of the images presented in Figures 3-4 show very good quality of the μCs in the DEM images compared to the ordinary mammography images. This visual conclusion is confirmed as well by the higher SC of the detected μCs on DEM images compared to the conventionally ones (Table 2). Considerable advantage of DEM technique is observed in the dense breast phantom. In the conventional mammograms, Figure 4a, the μCs are almost hidden in the breast tissue and difficult for detection. For fattier breast, one of the μCs was not visible at all on the ordinary image (Figure 3a), while another one may be recognized as a part of the gland tissue. On the DEM image (Figure 3b), all μCs are perfectly outlined due to the suppressed breast background.

Further improvement in the μCs visualization is observed using DTS and DEM-DTS technique. The

ISSN: 1727-1983

visual assessment of the tomograms displayed in Figures 3c, 4c lead to conclusion that DTS can bring in focus small μCs; thus giving an useful additional information for their dimension and location in the breast model. The same is valid for the DEM-DTS tomograms (Figures 3d, 4d), which demonstrate increased μCs visibility. DEM-DTS tomograms from non-filtered projections, as seen from these figures are blurred caused by out of focus structures overlaid in the tomosynthetic plane. Although the presented blur, the μCs are significantly outlined against the suppressed background. This was also confirmed by the significantly increased SC of the μCs detected on the DEM-DTS tomograms. The quality of the reconstructed tomograms may be enhanced using application of filtering to the initial synthetic projection data (with a ramp filter). These tomograms were not shown in this paper. However, the SC values for μC reconstructed from non-filtered DEM projections were approximately the same with those extracted from filtered DEM images. The later demonstrated improved μC visibility, compared to the results obtained with non-filtered projections.

Further on, the locations of the reconstructed μCs with DEM-DTS corresponded to their true locations in the breast phantom. This was shown through comparison of their z location in both the breast phantom and the reconstructed volume. Therefore, precise information can be extracted, including μC dimension and location characteristics.

Conclusions

The results showed the prominent advantage of using the DEM-DTS technique in 3D localising and visualising small μC in all types simulated breasts. Advantage of this combination is demonstrated for fatty and dense breasts. Precise dose calculations must be accomplished in future work. The three-dimensional reconstruction technique (DTS) contributed to the reconstruction of the volume of interest and to estimate the 3D locations and dimensions of the μC, while the dual-energy technique assisted in removing the structure breast tissue contrast.

References

[1] KERLIKOWSKE K., GRADY D., RUBIN S., SANDROCK C., and ERNSTER V. (1995): 'Efficacy of screening mammography. A meta-analysis', *JAMA,* **273,** pp. 149-154.

[2] JACKSON VP, HENDRICK RE, FEIG SA, and KOPANS DB 1993 Imaging of the radiographically dense breast *Radiology* 188**,** 297-301

[3] JOHNS P. and YAFFE M. (1985): 'Theoretical optimization of dual-energy x-ray imaging with application to mammography' *Med. Phys,* **12**, pp 289-296.

[4] JOHNS P., DROST D., YAFFE M. and FENSTER A. (1985): 'Dual-energy mammography: initial experimental results', *Med. Phys.*, **12**, pp. 297-304.

[5] CHAKRABORTY D. and BARNES G. (1989): 'An energy sensitive cassette for dual-energy mammography', *Med. Phys.*, **16**, pp. 7-13.

[6] BOONE J. (1991): 'Color mammography. Image generation and receiver operating characteristic evaluation' *Invest. Radiol.*, **26,** pp. 521-527.

[7] BRETTLE D. and COWEN A. (1994): 'Dual-energy digital mammography utilizing stimulated phosphor computed radiography', *Phys. Med. Biol.*, **39**, pp. 1989-2004.

[8] LEMACKS M., KAPPADATH S., SHAW C., LIU X. and WHITMAN G. (2002): 'A dual-energy subtraction technique for microcalcification imaging in digital mammography--a signal-to-noise analysis' *Med Phys.,* **29**, pp. 1739-1751.

[9] KAPPADATH S. and SHAW C. (2004): 'Quantitative evaluation of dual-energy digital mammography for calcification imaging' *Phys. Med. Biol.* **49**, pp. 2563-2576.

[10] NIKLASON L. T. et al (1997): 'Digital tomosynthesis in breast imaging', *Radiology*, **205**, pp. 399-406

[11] SURYANARAYANAN S., KARELLAS A., VEDANTHAM S., GLICK S. J., D'ORSI C. J., BAKER S. P. and WEBBER R. L. (2000): 'Comparison of tomosynthesis methods used with digital mammography', *Acad. Radiol.*, **7**, pp. 1085-97

[12] WU T., STEWART A., STANTON M., MCCAULEY T., PHILLIPS W., KOPANS D. B., MOORE R. H., EBERHARD J. W., OPSAHL-ONG B., NIKLASON L. and WILLIAMS M. B. (2003): 'Tomographic mammography using a limited number of low-dose cone-beam projection images' *Med. Phys.*, **30**, pp. 365-380

[13] SONE S., KASUGA T., SAKAI F., OGUCHI K., ITOH A., LI F., MARUYAMA Y., KUBO K., HONDA T., HANIUDA M., and TAKEMURA K. (1996): 'Digital tomosynthesis imaging of the lung', *Radiat. Med.*, **14,** pp. 53-63.

[14] LIU J., NISHIMURA D., and MACOVSKI A. (1987): 'Vessel imaging using dual-energy tomosynthesis' *Med. Phys.*, **14**, pp. 950-955.

[15] BLIZNAKOVA K., BLIZNAKOV Z., BRAVOU V., KOLITSI Z., and PALLIKARAKIS N. (2003): 'A 3D breast software phantom for mammography simulation', *Phys. Med. Biol.*, **22**, pp. 3699-3720.

[16] ERGUN D. et al (1990): 'Single-exposure dual-energy computed radiography: improved detection and processing' *Radiology* **174** pp. 243-249.

[17] KOLITSI Z., PANAYOTAKIS G., ANASTASSOPOULOS V., SKODRAS A., and PALLIKARAKIS N. (1992): 'A multiple projection algorithm for digital tomosynthesis', *Med. Phys.*, **19**, pp. 1045-1050.

ISSN: 1727-1983